

A numerical study of a natural convection flow in a cavity

Yanhu Guo¹ and Klaus-Jürgen Bathe^{2,*},[†]

¹*ADINA R & D, Inc., 71 Elton Ave., Watertown, MA 02472, U.S.A.*

²*Department of Mechanical Engineering, Massachusetts Institute of Technology, Cambridge, MA 02139, U.S.A.*

SUMMARY

The solution to a benchmark problem of a differentially heated cavity flow with $Ra=3.4 \times 10^5$ and $Pr=0.71$ was solicited for presentation at a special session entitled ‘Computational Predictability of Natural Convection Flows in Enclosures’ which was held at the First MIT Conference on Computational Fluid and Solid Mechanics. The objective of this paper is to present the results obtained using the ADINA System.

The 9-node quadrilateral element in ADINA was used with various meshes. Periodic solutions with a period of 3.42–3.43 were obtained. Compared with the average values of the solution variables and the periods, the calculated amplitudes of the periodic solutions were found to be more sensitive to the spatial and temporal discretizations used. The flow patterns, such as boundary layers, vortices, etc. were also studied using a fine 40×120 element mesh. Vortices and their evolutions were revealed inside the periodic flow field. Copyright © 2002 John Wiley & Sons, Ltd.

KEY WORDS: natural convection; unsteady cavity flow; ADINA

1. INTRODUCTION

The solution of a differentially heated cavity flow at near-critical Rayleigh number was solicited (see Reference [1]) for presentation at a special session entitled ‘Computational Predictability of Natural Convection Flows in Enclosures’ which was held at the First MIT Conference on Computational Fluid and Solid Mechanics [2]. Studies of such flows have been of interest for a long time [3, 4], but solving this benchmark problem accurately still provides a challenge.

The ADINA System is a finite element program system which has been widely used to perform comprehensive analyses of structures, fluid flows, and fluid–structure interactions. Incompressible flows, slightly compressible flows and fully compressible flows at high Mach number can be solved. The objective of this paper is to present the results

*Correspondence to: K. J. Bathe, Department of Mechanical Engineering, Massachusetts Institute of Technology, Cambridge, MA 02139, U.S.A.

[†]E-mail: kjb@mit.edu

Received 31 December 2001

Revised 1 July 2002

obtained in the analysis of the benchmark problem using the incompressible flow assumptions in ADINA.

2. STATEMENT OF THE PROBLEM AND NUMERICAL PROCEDURES

A brief description of the problem is given in Figure 1. More details can be found in Reference [1]. The governing Navier–Stokes equations to be solved for this problem are

Continuity:

$$\rho_0 \nabla \cdot \mathbf{v} = 0 \quad (1)$$

Momentum:

$$\rho_0 \frac{\partial \mathbf{v}}{\partial t} + \rho_0 (\mathbf{v} \cdot \nabla) \mathbf{v} = -\nabla p + \nabla \cdot (2\mu \mathbf{e}) + \rho_0 \mathbf{g} [1 - \beta(\theta - \theta_0)] \quad (2)$$

Energy:

$$\rho_0 C_v \frac{\partial \theta}{\partial t} + \rho_0 C_v (\mathbf{v} \cdot \nabla) \theta = \nabla \cdot (k \nabla \theta) \quad (3)$$

where \mathbf{v} , p , θ , \mathbf{e} , μ , k , C_v , ρ_0 , θ_0 , β , \mathbf{g} are the velocity vector, pressure, temperature, velocity strain tensor, viscosity coefficient, heat conductivity, specific heat at constant volume, reference density, reference temperature, thermal coefficient of expansion and gravitational acceleration vector. Of course, t denotes time.

The boundary conditions for the variables are

$$\text{at } x=0: \quad \mathbf{v} = \mathbf{0}, \quad \theta = 0.5 \quad (4a)$$

$$\text{at } x=W: \quad \mathbf{v} = \mathbf{0}, \quad \theta = -0.5 \quad (4b)$$

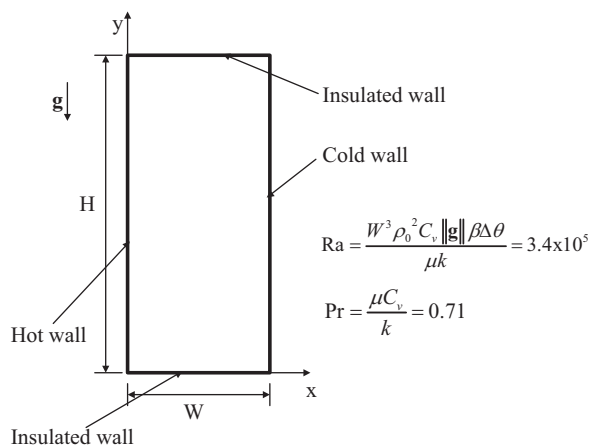


Figure 1. Schematic of the benchmark problem.

$$\text{at } y=0: \quad \mathbf{v}=\mathbf{0}, \quad \frac{\partial \theta}{\partial y}=0 \tag{4c}$$

$$\text{at } y=H: \quad \mathbf{v}=\mathbf{0}, \quad \frac{\partial \theta}{\partial y}=0 \tag{4d}$$

$$\text{at } x=0: \quad y=0, \quad p=0 \tag{4e}$$

where W and H denote the width and the height of the enclosure, respectively. We shall later use $\Delta\theta = \theta|_{x=0} - \theta|_{x=W}$.

The initial conditions are,

$$\text{at } t=0: \quad \mathbf{v}=\mathbf{0}, \quad \theta=0, \quad p=0 \tag{5}$$

The numerical methods used in the ADINA System to solve these equations are presented in References [5, 6]: The finite element solution for incompressible flows is based on a weak form of the Navier–Stokes equations using the Galerkin procedure. The continuity equation, the momentum equations and the energy equation are weighted with the virtual quantities of pressure, velocities, and temperature, respectively. Of course, it is critical to use effective finite element discretization schemes, time integration methods, and solution schemes for the set of algebraic equations. We discuss the techniques used in the problem solution considered here in the next section.

3. MODEL SET-UP

The ADINA System offers solution capabilities for various forms of governing fluid flow equations and in very complex geometries [6]. In this study, a two-dimensional incompressible flow with heat transfer is assumed to take place. A constant material model is used and the material parameters are chosen (see Table I) to make the Rayleigh number equal to 3.4×10^5 and the Prandtl number equal to 0.71, as requested. The wall boundary condition is applied to all four walls for the velocity and pressure. The temperature is prescribed at the two side

Table I. Material and geometry parameters.

Variable	Value
ρ_0	1.0
μ	0.71
k	1.0
C_v	1.0
β	2.414×10^5
$\ \mathbf{g}\ $	1.0
θ_0	0.0
$\Delta\theta$	1.0
W	1.0
H	8.0

walls to model the differential heating. The adiabatic condition for the temperature is a natural boundary condition and is applied to the horizontal top and bottom walls. The pressure at the bottom-left corner is fixed to be zero. The initial conditions are zero velocity, zero pressure and zero temperature, see Equation (5).

3.1. Spatial discretization of the computational domain

Three different elements are available for two-dimensional fluid flow simulations in the ADINA System; namely, a 3-node triangular, a 6-node triangular and a 9-node quadrilateral element (9/4-c or Q_2-Q_1 element [5]). The last two elements are based on parabolic velocity interpolations while the first one is based on a linear interpolation (plus a bubble). All elements satisfy the inf-sup condition for incompressible analysis which means that they are stable and optimal, i.e. the order of error in the spatial discretization is the smallest possible [5, 7]. Since this benchmark problem is very sensitive to numerical errors and because the computational domain is rectangular, the 9-node quadrilateral element was used for all simulations. Note that the 9-node element requires more memory and CPU time than does the 3-node triangular element.

Four different meshes have been used to solve the benchmark problem with the element grading for the meshes as follows: mesh 1, 20×100 elements which was suggested in Reference [1]; mesh 2, 24×100 elements; mesh 3, 30×100 elements, and mesh 4, 40×120 elements. We note that a more natural way to establish a finer mesh is to double the number of elements in both directions. However, this approach would lead to rather long solution times. Instead, we first increased the number of elements into the x -direction and then also used one mesh with an increased number of elements in both directions.

The non-uniform meshes were constructed on 16 surfaces (see Figure 2). These surfaces ensured that the five hard points (see Figure 2, defined in Reference [1]) at which the compulsory time-history data is to be computed are always node points in the different grid discretizations. The minimum element size of each mesh was: mesh 1, $\Delta x = 0.01725$, $\Delta y = 0.02987$; mesh 2, $\Delta x = 0.01483$, $\Delta y = 0.02987$; mesh 3, $\Delta x = 0.0125$, $\Delta y = 0.02987$; mesh 4, $\Delta x = 0.005$ and $\Delta y = 0.01$. Note that the minimum element size in the finest mesh was about $\frac{1}{3}$ rd that of the coarsest mesh although the number of element layers was only doubled in the x -direction and only increased by 20 per cent in the y -direction.

3.2. Time integration scheme and time step size

The α time integration method [5] is employed in the ADINA System for transient fluid flow simulations. With the value 0.5 for the time integration parameter α , the trapezoidal rule is used with an accuracy of second order in time. In this study, we employed $\alpha = 0.505$ from time zero to the time at which a periodic solution is measured. Then the value of α was changed to 0.5. The reason for using first a value different from 0.5 was that then better convergence in the Newton-Raphson iterations was achieved.

To choose the time step size, we considered the time constant used for this problem $W/\sqrt{g\beta W\Delta\theta}$, $g = \|\mathbf{g}\|$, (see Reference [1]), which in our model set-up gives a value of 0.00203531 (to six digits). As a first guess for the time step size, we employed the value 0.0002, which is about $\frac{1}{10}$ th of the time constant. Based on the simulation using the coarsest

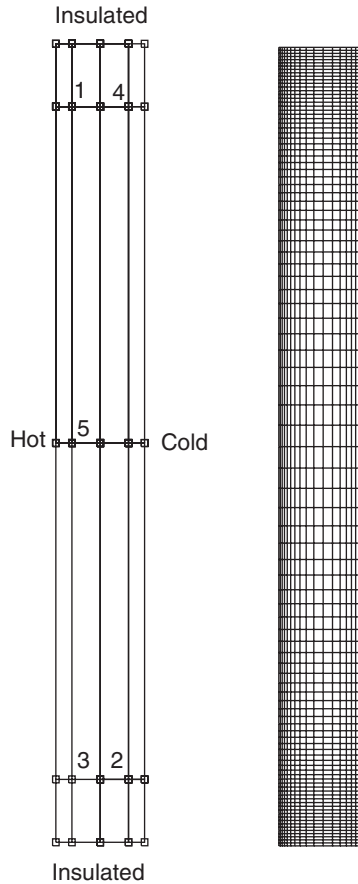


Figure 2. Geometry and a typical mesh (the 20×100 element mesh).

mesh, we found that there were about 34 time steps per time period of oscillations. Hence, we kept this time step size for all simulations.

3.3. Convergence criterion for iterations

The time-stepping solution requires that a set of non-linear equations be solved at each time considered. To solve these equations ADINA provides two options, the Newton–Raphson method and the successive substitution method. The Newton–Raphson method was used for all simulations in this study. The linear equations, which are established in the Newton–Raphson method, were solved using a sparse direct solver. Of course, a convergence criterion needs to be used to stop the iterations. In all simulations of this study, the stopping criterion used was that the (Euclidean) norm of the incremental solution variables divided by the norm of the current values of these variables was smaller than 10^{-9} . The convergence histories showed that generally only three iterations were needed in each time step.

Table II. Characteristic values used for non-dimensionalization.

Variable	Characteristic value	
	Formulation	Quantity
Heat conductivity	k	1.0
Length	W	1.0
Time	$W/\sqrt{g\beta W\Delta\theta}$	0.00203531
Density	ρ_0	1.0
Temperature	$\Delta\theta$	1.0
Velocity	$\sqrt{g\beta W\Delta\theta}$	491.325
Pressure	$\rho_0 g\beta W\Delta\theta$	2.414×10^5
Stream function	$W\sqrt{g\beta W\Delta\theta}$	491.325
Vorticity	$\sqrt{g\beta W\Delta\theta}/W$	491.325

4. RESULTS AND EVALUATION

The solution results comprise the required data and additional results that we choose to also report upon. Note that all the results presented hereafter are non-dimensionalized as described in Reference [1] except where it is emphasized. For completeness, the characteristic values of all the variables used, and for which results are given, are listed in Table II.

4.1. Compulsory results

The time histories of the temperature at point 1 are shown in Figure 3 for the four meshes. Figure 4 shows the same time histories on an expanded scale. The time histories show that periodic solutions are obtained for all simulations using the different mesh densities.

The compulsory point, wall and global solution results are tabulated in Table III. In the table the following notation is used:

Ave.	the average of a variable over a period of oscillation within the sample used
Amp.	the difference between the maximum and the minimum of a variable over a period of oscillation within the sample used
Period	the time duration for a period of oscillation of a variable within the sample used
u_1	the x -direction velocity component at point 1
v_1	the y -direction velocity component at point 1
θ_1	the temperature at point 1
ε_{12}	skewness (see Reference [1]), the summation of the temperature at points 1 and 2
Ψ_1	the stream function at point 1; $u = \partial\Psi/\partial y$, $v = -\partial\Psi/\partial x$, $\Psi = 0$ at the walls
ω_1	the vorticity at point 1; $\omega = \partial v/\partial x - \partial u/\partial y$
ΔP_{ij}	the pressure difference between point i and point j ; $\Delta P_{ij} = p_i - p_j$
$Nu _{x=0,W}$	the wall Nusselt number at $x=0$ or W ; $((1/H)(W/\Delta\theta) \int_0^H \partial\theta/\partial x _{x=0,W} dy)$

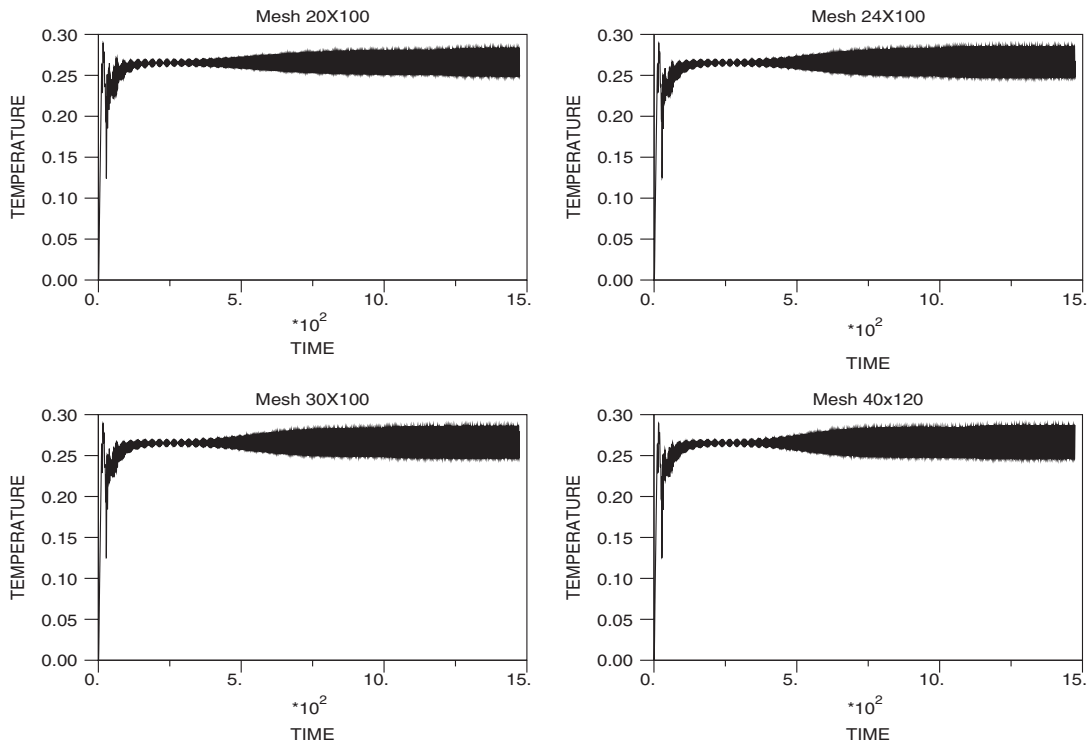


Figure 3. Time history of temperature at point 1.

- \hat{u} the ‘average’ velocity metric over the whole enclosure requested in Reference [1]
 $(= \sqrt{(1/2HW) \int_0^H \int_0^W \mathbf{v} \cdot \mathbf{v} \, dx \, dy})$
- $\hat{\omega}$ the ‘average’ vorticity over the whole enclosure requested in Reference [1]
 $(= \sqrt{(1/2HW) \int_0^H \int_0^W \omega^2 \, dx \, dy})$

As for the samples used for all simulations, the average, the amplitude (one-half the peak-to-valley amplitude), and the period in Table III, were measured during the last 1000 time steps (corresponding to a duration of approximately 98 time units).

Note that both the average and the amplitude of the skewness ε_{12} were found to be around 10^{-9} which is as small as the stopping criterion in the Newton–Raphson iterations. This implies that the temperature field is skew-symmetric.

4.2. Computational resource used

All simulations were performed on a serial computer using ADINA 7.4 with the following capacity:

- Machine: IBM RS/6000 44P Model 170.
- Total memory: 512 MB.

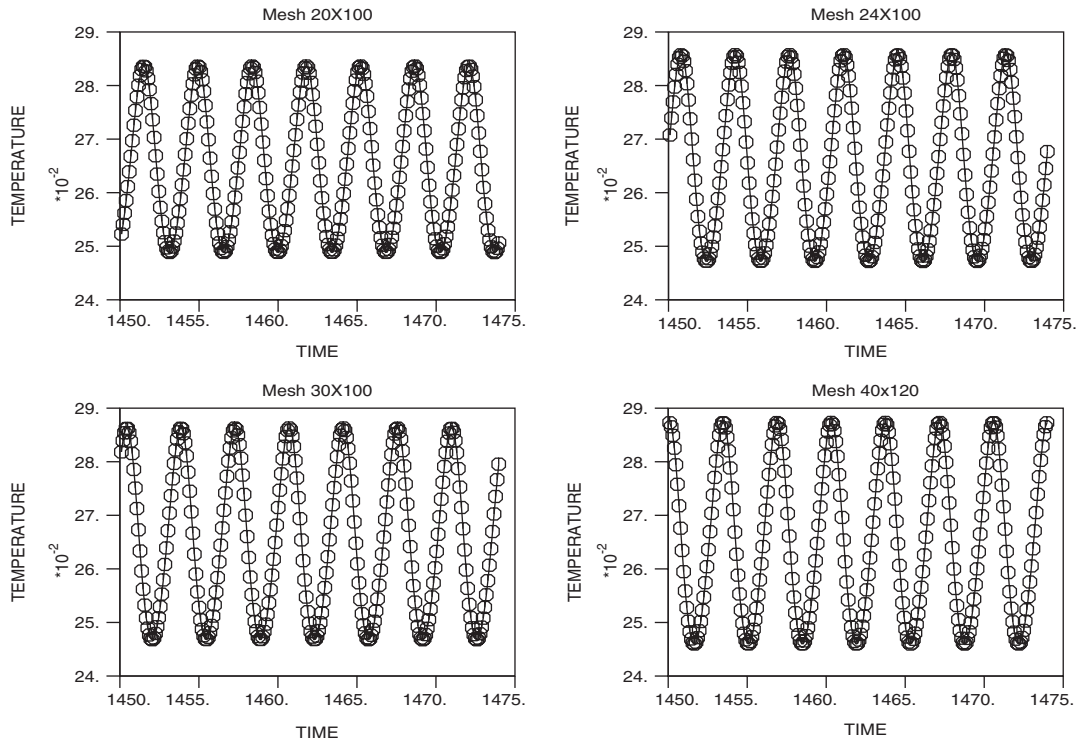


Figure 4. Time history of temperature at point 1 on expanded scale.

- Number of the processors: 1.
- Memory used for four grids [MB]: 63.1, 77.8, 102.9, 174.7.
- CPU time used for four grids [ms/node/time step]: 1.21, 1.13, 1.30, 1.58.

4.3. The effect of the mesh density

Referring to Table III, we can make the following observations:

- (1) Considering ε_{12} , both the average value and the amplitude decrease as the mesh density increases.
- (2) Considering all other compulsory data, we note that:
 - The calculated average values and periods do not change any more significantly as the finest mesh is reached.
 - The calculated amplitudes, however, still change by about 5 per cent between the 30×100 element mesh results and the 40×120 element mesh results.

This observation tells that the averages and periods have probably been predicted quite accurately. But if the objective is to predict the amplitudes more accurately, a finer mesh may still be needed.

Table III. Compulsory point, wall and global solution results.

Quantity	Mesh of 20 × 100 elements			Mesh of 24 × 100 elements		
	Ave.	Amp.	Period	Ave.	Amp.	Period
u_1	0.5439e-1	0.4406e-1	3.425	0.5558e-1	0.4908e-1	3.422
v_1	0.4618	0.6450e-1	3.425	0.4622	0.7052e-1	3.425
θ_1	0.2653	0.3506e-1	3.425	0.2655	0.3858e-1	3.425
ε_{12}	0.1322e-8	0.5232e-7	3.425	0.1288e-8	0.4734e-7	3.425
Ψ_1	-7.427e-2	0.5674e-2	3.428	-7.406e-2	0.6270e-2	3.425
ω_1	-2.556	0.8816	3.425	-2.4908	0.9814	3.425
ΔP_{14}	-2.116e-3	1.7196e-2	3.425	-2.068e-3	1.8794e-2	3.425
ΔP_{31}	-0.5348	1.9112e-2	3.428	-0.5349	0.2080e-1	3.422
ΔP_{35}	0.5369	0.8652e-2	3.428	0.5369	0.9438e-2	3.425
$Nu _{x=0}$	4.5782	0.5918e-2	3.425	4.5788	0.6462e-2	3.425
$Nu _{x=w}$	4.5783	0.5920e-2	3.425	4.5788	0.6462e-2	3.425
\hat{u}	0.2393	0.2852e-4	3.425	0.2394	0.3112e-4	3.422
$\hat{\omega}$	3.0175	0.2704e-2	3.425	3.0174	0.2944e-2	3.425

Quantity	Mesh of 30 × 100 elements			Mesh of 40 × 120 elements		
	Ave.	Amp.	Period	Ave.	Amp.	Period
u_1	0.5572e-1	0.5052e-1	3.425	0.5610e-1	0.5294e-1	3.422
v_1	0.4619	0.7204e-1	3.422	0.4620	0.7512e-1	3.422
θ_1	0.2656	0.3950e-1	3.422	0.2654	0.4134e-1	3.425
ε_{12}	0.818e-9	0.4166e-7	3.425	0.285e-9	0.2250e-8	3.417
Ψ_1	-7.391e-2	0.6470e-2	3.422	-7.385e-2	0.6768e-2	3.421
ω_1	-2.4425	1.0036	3.422	-2.4334	1.057	3.425
ΔP_{14}	-1.883e-3	1.9158e-2	3.425	-2.003e-3	0.2004e-1	3.421
ΔP_{31}	-0.5351	0.2122e-1	3.425	-0.5349	0.2208e-1	3.422
ΔP_{35}	0.5370	0.9644e-2	3.425	0.5369	0.9976e-2	3.422
$Nu _{x=0}$	4.5791	0.6598e-2	3.422	4.5795	0.6892e-2	3.422
$Nu _{x=w}$	4.5791	0.6600e-2	3.422	4.5795	0.6890e-2	3.422
\hat{u}	0.2394	0.3198e-4	3.422	0.2395	0.3278e-4	3.425
$\hat{\omega}$	3.0174	0.3004e-2	3.422	3.0172	0.3116e-2	3.425

4.4. The effect of changing α

As mentioned above, when α equals to 0.5, the time integration method is second-order accurate. Figure 5 shows the effect of changing α from the value 0.505 to 0.5 on the temperature history at point 1 using the mesh of 40 × 120 elements. The change in α is imposed to occur at time equal to 1080.91. It can be seen that the amplitude of the temperature oscillation increases after the change of α .

4.5. Additional results

In this section additional computed data are given, but only the results using the finest mesh of 40 × 120 elements are considered.

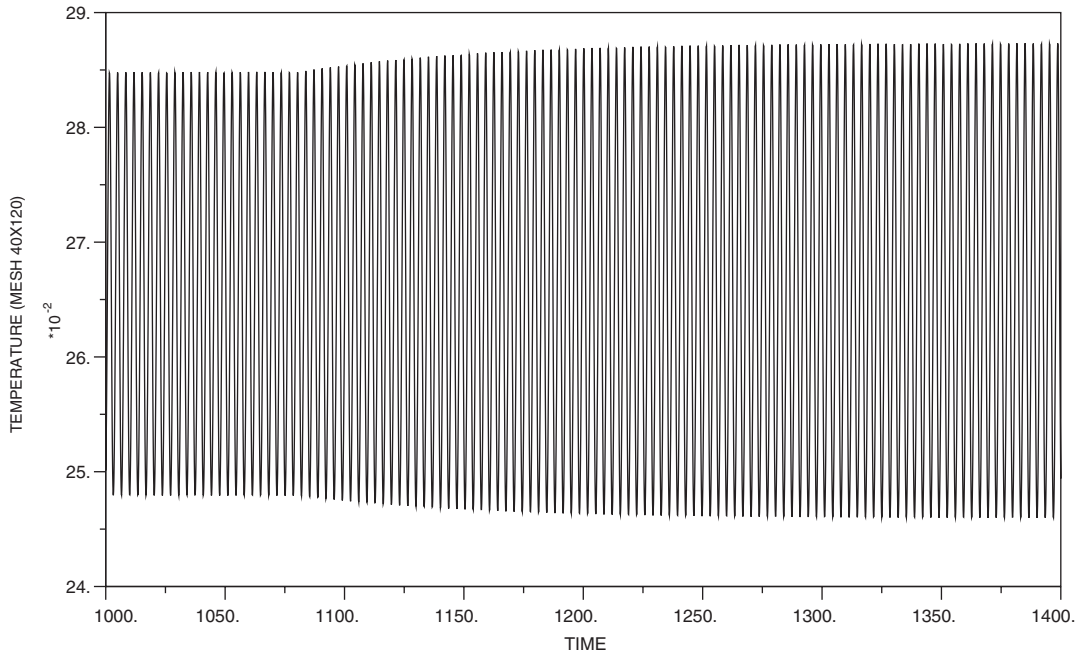


Figure 5. The effect of α (α changes from 0.505 to 0.5 at time=1080.91).

4.5.1. Time histories at other hard points. Figure 6 shows the time histories of temperature, pressure and the two velocity components in one time period at different hard points. The results reveal that the variations of temperature, and the two velocity components are nearly anti-symmetric between points 1 and 2 and between points 3 and 4. The pressure difference (assuming the pressure at point 5 to be equal to zero) also shows anti-symmetry between points 1 and 3.

4.5.2. Spatial distributions and vortex evolutions. The spatial distributions of temperature and velocity components at four time points along the horizontal and the vertical center lines of the cavity are shown in Figures 7 and 8, separately. These time points correspond to the times 0, $T/4$, $T/2$ and $3T/4$, where T is the period of oscillation. The v -component of velocity is shown along the horizontal center line in Figure 7 while the u -component of velocity is shown along the vertical center line in Figure 8. The boundary layers for the velocities and temperature can be observed clearly. As expected, the thermal boundary layer is thicker than the velocity boundary layer. Also note that the differences in the temperature and velocity components for the different time points considered are very small along the centre lines.

To obtain a view of the whole flow field, the contours of temperature, pressure, total velocity and the stream function at the non-dimensional time equal to 1476.9 are shown in Plate 1. Note that the time shown in the contour legend is a dimensional time (the time constant is 0.00203531, see Table II). The flow patterns including the boundary layers and vortices can be seen clearly.

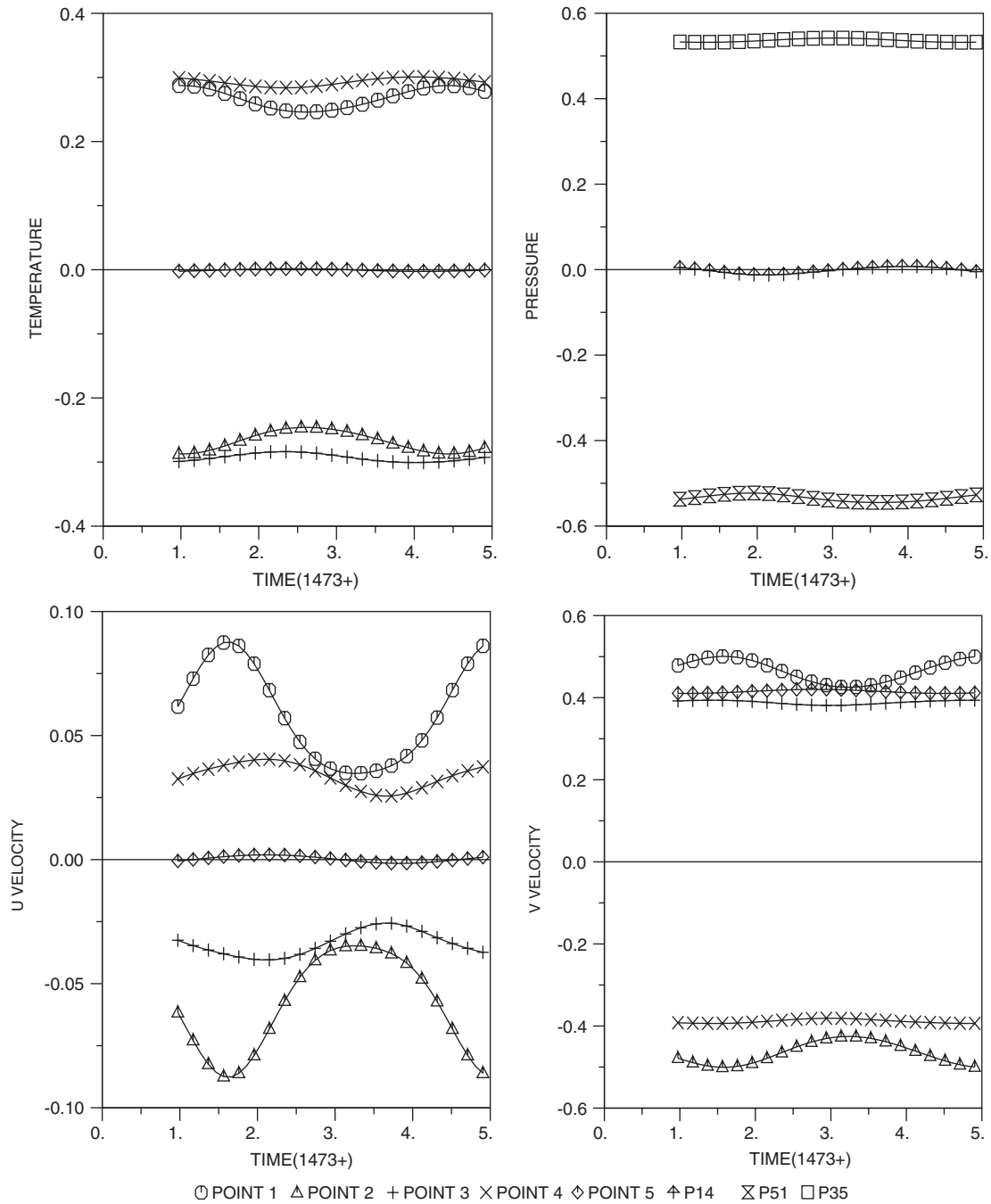


Figure 6. Time histories at other hard points (the actual time is obtained by adding 1473 to the time shown).

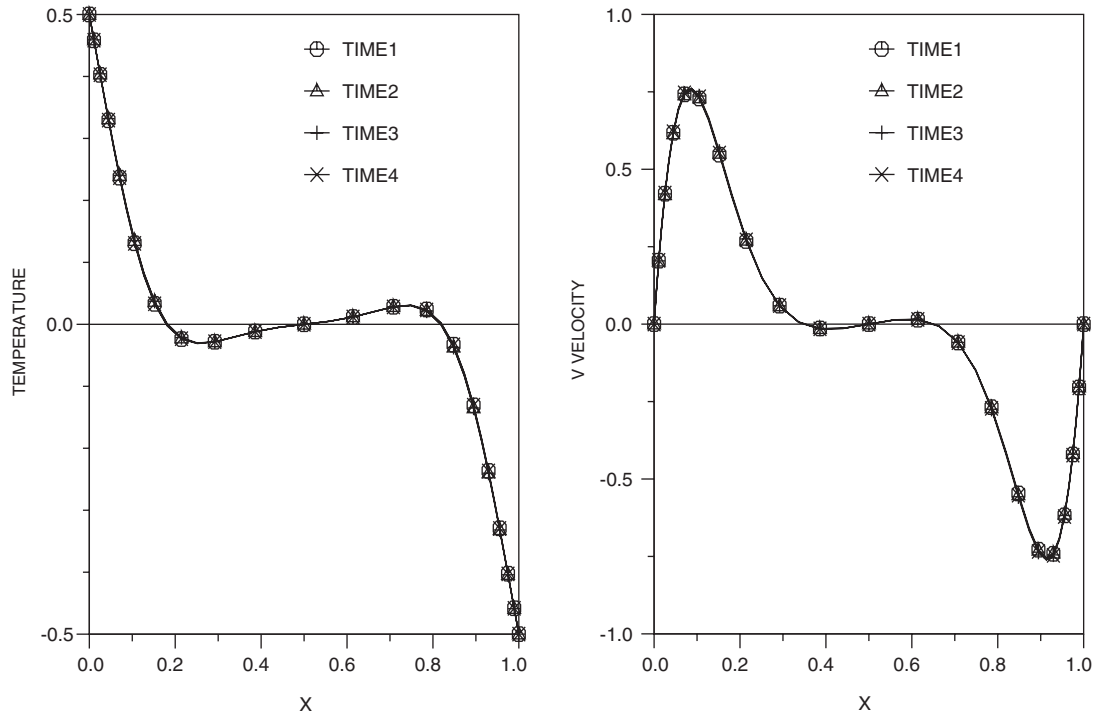


Figure 7. Temperature and velocity distributions along the horizontal centre line.

To show the vortex evolution inside the cavity, the streamlines at 10 equally spaced time points corresponding to one time period are shown in Plate 2. It can be seen that two major vortices are located near the top and bottom walls. Both vortices rotate clockwise. Between these two major vortices, there is one large vortex. Inside this vortex, there is a more complex vortex pattern. The decrease and increase of the strengths of the two smaller vortices, which are located inside the large vortex, with time, can be seen in the figure.

5. CONCLUDING REMARKS

The solutions of a benchmark problem of cavity flow near the critical Rayleigh number have been obtained using the ADINA System. The results presented in the paper include the compulsory results and some additional results. The compulsory results including the point data, wall data and global data have been computed for four meshes. The flow patterns including the boundary layers and vortices were also studied based on the results obtained with the finest mesh of 40×120 9-node elements.

Periodic solutions with a period of 3.42–3.43 were obtained in all simulations. Compared with the averages of the various solution variables and the periods, the amplitudes of the periodic solutions are more sensitive to the spatial and temporal discretizations used. Based on

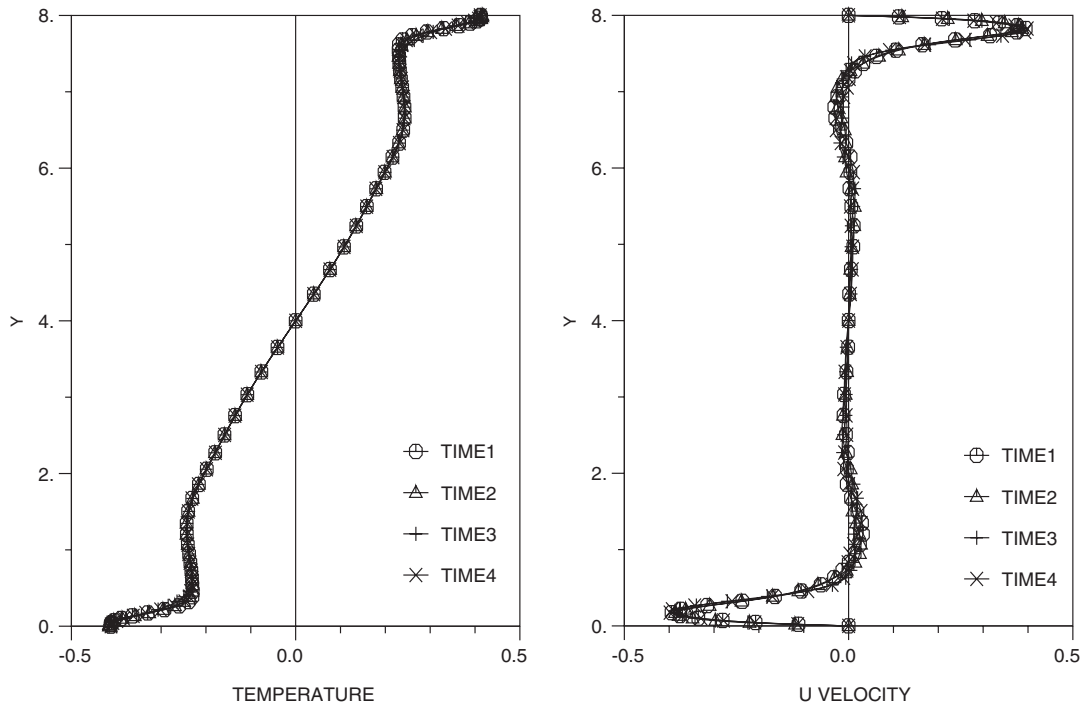


Figure 8. Temperature and velocity distributions along the vertical centre line.

the study performed and the solution schemes used, we believe that quite accurate predictions for certain solution quantities (such as average values and periods) have been obtained.

REFERENCES

1. Christon MA, Gresho PM, Sutton SB. Computational predictability of natural convection flows in enclosures. *International Journal for Numerical Methods in Fluids* 2002; **40**:953–980.
2. Bathe KJ (ed), Computational fluid and solid mechanics. *Proceedings of the First MIT Conference on Computational Fluid and Solid Mechanics*. Elsevier Science: Amsterdam, 2001.
3. Minkowycz WJ, Sparrow EM, Schneider GE, Pletcher RH. *Handbook of Numerical Heat Transfer*. Wiley: New York, 1988.
4. Le Quéré P. Accurate solutions to the square thermally driven cavity at high Rayleigh number. *Computers and Fluids* 1991; **20**:29–41.
5. Bathe KJ. *Finite Element Procedures*. Prentice Hall: Englewood Cliffs, NJ, 1996.
6. ADINA R&D, Inc. *ADINA Theory and Modeling Guide, vol. III: ADINA-F*, August 2000.
7. Bathe KJ. The inf–sup condition and its evaluation for mixed finite element methods. *Computers and Structures* 2001; **79**:241–252, 971.

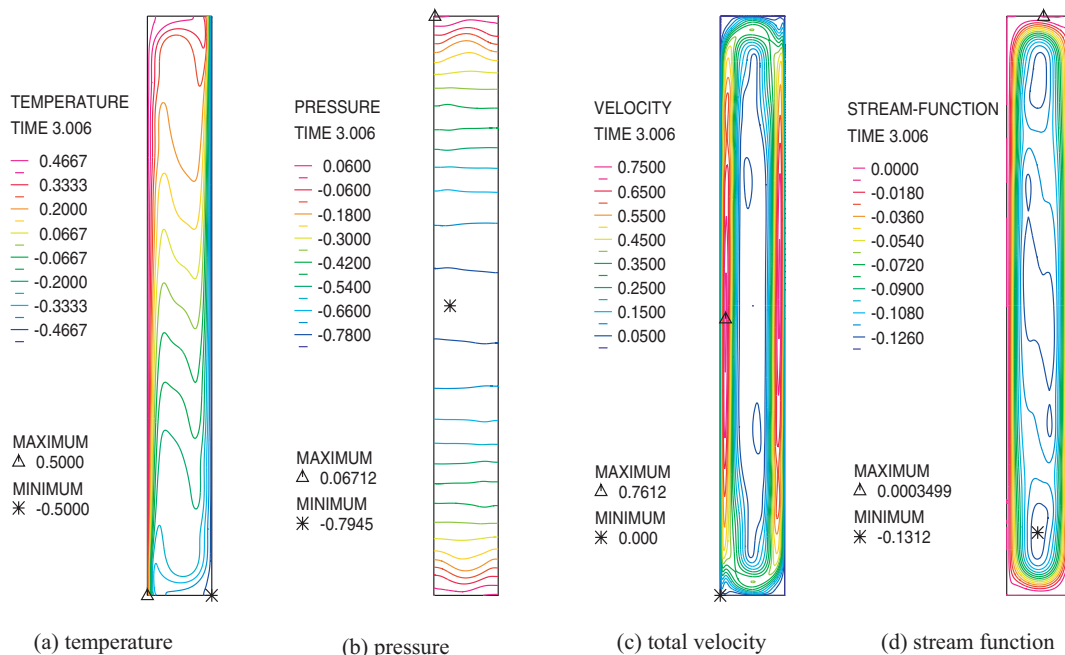


Plate 1. Contours of calculated variables at time 1476.9 for the 40×120 element mesh: (a) temperature; (b) pressure; (c) total velocity and (d) stream function.

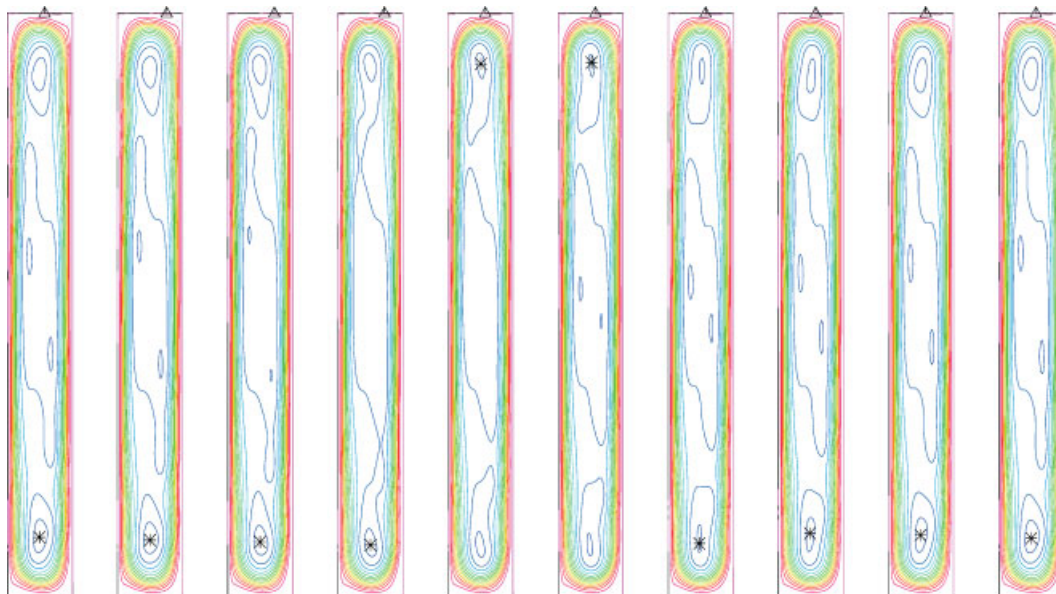


Plate 2. Streamlines at ten time points within a period. The 10 time points correspond to 10 equal intervals in time.